Available online at www.sciencedirect.com
ScienceDirect
International Journal of Heat and Mass Transfer 50 (2007) 4166–4179
International Journal of HEAT and MASS TRANSFER
www.elsevier.com/locate/ijhmt

The effects of buoyancy on the performance of a PEM fuel cell with a wave-like gas flow channel design by numerical investigation

Jenn-Kun Kuo, Cha'o-Kuang Chen *

Department of Mechanical Engineering, National Cheng Kung University, Tainan 70101, Taiwan

Received 10 January 2007; received in revised form 24 February 2007
Available online 8 May 2007

Abstract

This study performs numerical simulations to investigate the effects of buoyancy on the gas flow characteristics, temperature distribution, electrochemical reaction efficiency and electrical performance of a proton exchange membrane fuel cell (PEMFC) with a novel wave-like gas flow channel design. In general, the simulation results show that compared to the straight geometry of a conventional gas flow channel, the wave-like configuration enhances the transport through the porous layer and improves the temperature distribution within the channel. As a result, the PEMFC has an improved fuel utilization efficiency and an enhanced heat transfer performance. It is found that the buoyancy effect increases the velocity of the reactant fuel gases in both the vertical and the horizontal directions. This increases the rate at which the oxygen gas is consumed in the fuel cell but improves the electrical performance of the PEMFC. The results show that compared to the conventional straight gas flow channel, the wave-like gas flow channel increases the output voltage and improves the maximum power density by approximately 39.5%.

Keywords: PEMFC; Buoyancy effect; Wave-like gas flow channel

1. Introduction

Due to their low operating temperature and high energy efficiency, proton exchange membrane fuel cells (PEMFCs) are regarded as a viable power source for a variety of applications. Various PEMFC models have been presented in the literature in recent years. Bernardi and Verbrugge [1,2] and Springer [3] proposed one-dimensional models as a basic platform for more advanced PEMFC modeling. The two-dimensional models presented by Nguyen and White [4] assumed that the transport of oxygen into the catalyst layer occurred solely as a result of diffusion. However, the effects of the gas diffusion layer (GDL) morphology and the gas flow field structure on the diffusion mechanism were not considered and hence the practical applicability of these models was somewhat limited. Recent years have witnessed a considerable increase in the power densities, reliability and electrical performance of PEMFCs. However, the underlying physics involved in the operation of a PEMFC are highly complex and are poorly understood. Accordingly, an increasing number of researchers have employed computational fluid dynamics (CFD) simulations to model PEMFCs in order to obtain a fuller understanding of their fluid flow structures, heat and mass transfer characteristics, and electrochemical reaction efficiency.

Various gas flow channel configurations have been proposed for PEMFC applications, including serpentine channels, multiple parallel channels, interdigitated channels, and so forth. In conventional PEMFCs with straight gas flow channels, the reactant gases diffuse into the catalyst layer through the gas diffusion layer. However, the diffusion process is inherently slow, and hence the electrical performance of such PEMFCs is limited. In an attempt to overcome this problem, Kuo and Chen [5–7] proposed a novel PEMFC design in which the surfaces of the gas flow channels were configured with a wave-like structure. The

* Corresponding author. Tel.: +886 6 2757575x62140; fax: +886 6 2342081.
E-mail address: ckchen@mail.ncku.edu.tw (C.-K. Chen).

0017-9310/$ - see front matter © 2007 Elsevier Ltd. All rights reserved.
doi:10.1016/j.ijheatmasstransfer.2007.02.039

Nomenclature

C	mass fraction
C_F	quadratic drag factor
D	mass diffusion (m^2/s)
F	Faraday's constant (96485 C/mol)
g	gravity acceleration (9.81 m/s^2)
i_e	current density (A/m^2)
i_m	ionic current density (A/m^2)
j	transfer current density (A/m^{-3})
k_c	condensation rate constant (1/s)
k_e	evaporation rate constant (1/atm s)
k_m^{eff}	effective ionic conductivity of membrane (S/cm)
k_s^{eff}	elective electric conductivity of the GDL (S/cm)
k_p	permeability (m^2)
M	molecular weight (kg/mol)
n	charge number of the sulfonic acid ions
P	pressure (atm)
R	universal gas constant (8.314 J/mol k)
S	source term
T	temperature (K)
u	velocity in the x-direction (m/s)
v	velocity in the y-direction (m/s)
V	operating voltage (V)
Z_f	spices valence

Greek symbols

α	transfer coefficient for the reaction
β	coefficient of thermal expansion
ε	porosity
λ	water content of membrane
ρ	density (kg/cm^2)
σ	ionic conductivity ($1/\Omega$ m)
τ	tortuosity
υ	viscosity of flow (kg/m s)
Φ	phase potential (V)
η_{act}	activation overpotential (V)

Subscripts

a	anode
c	cathode
CL	catalyst layer
e	energy
eff	effective
GDL	gas diffusion layer
h_1	gas flow channel height
h_2	gas diffusion channel height
in	inlet
k	kth component of fuel reactant
m	membrane phase
mem	membrane
out	outlet, outer
ref	reference
w	wall
x	X-direction
y	Y-direction

numerical results revealed that this unique channel design improved the uniformity of the velocity and temperature distributions within the channel and reduced the included angle between the dimensionless velocity vector and the temperature gradient thereby improving the heat transfer characteristics of the fuel cell.

This study performs a series of numerical simulations to investigate the effect of the buoyancy force [8–10] in a wave-like gas flow channel on the velocity, temperature and gas concentration distributions within the channel. The results for the wave-like gas flow channel are compared with those obtained for a conventional straight channel. The reactant fuel consumption and electrical performance of a PEMFC with a wave-like gas flow channel are then evaluated both with and without buoyancy effects. Again, the results are compared with those obtained for a straight gas flow channel.

2. Simulation model

The simulations performed in this study are based on a steady state, single-phase, multi-species, two-dimensional mass transfer model of a PEMFC. Fig. 1 presents a 3D solid-rendered illustration of the fuel cell. As shown, the major components of the PEMFC include: (1) anode and cathode flow channels, both with wave-like profiles; (2) two carbon paper gas diffusion layers; (3) two catalyst layers; and (4) a proton exchange membrane. The geometric and physical parameters applied in the simulations are summarized in Table 1. Note that some minor parameters are omitted from this table, but can be found in the literature [11–19]. The operating pressure and temperature are assumed to be 1 atm and 323 K, respectively. Regarding the reactant gases, the anode is supplied with humidified hydrogen with a mass fraction of 70/30% H_2/H_2O and the cathode side is fed with saturated oxygen with a mass fraction of 21/79% O_2/N_2. The N_2 gas is considered to be inert and serves as a diluent. When the reactant gases flow in the gas channels of the PEMFC, they are subject to a mixed convection effect, i.e., natural convection [20–22] as a result of the elevated temperature in the gas flow channel and forced convection as a result of the wave-like profile of the channel walls. The simulations are performed both with and without the effects of the buoyancy force (i.e., the convective effect) acting on the gases taken into consideration. The buoyancy effect is modeled by varying the density of the oxygen and hydrogen gases in direct proportion to the temperature when calculating the body force term (i.e., the buoyancy effect).

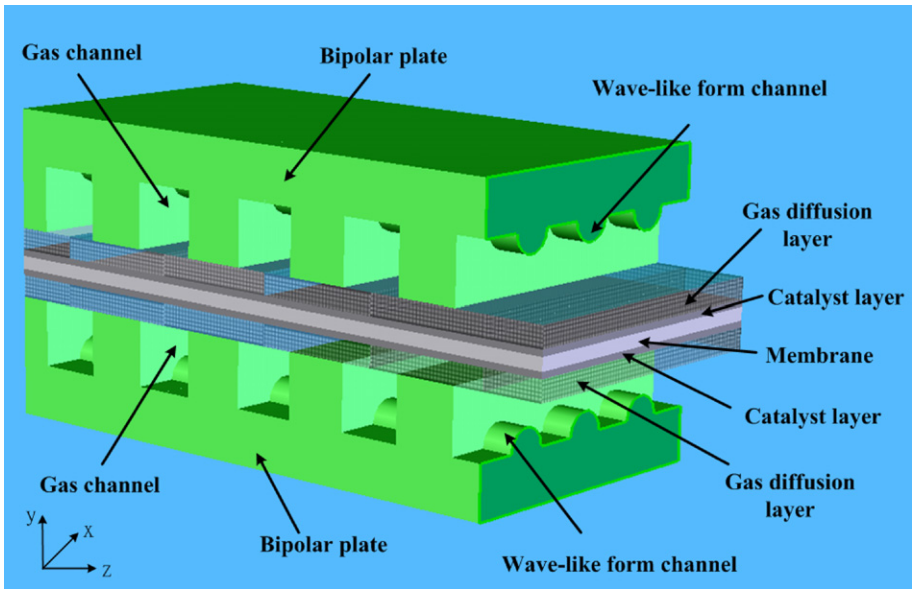

Fig. 1. Schematic representation of PEMFC with wave-like gas flow channel.

Table 1
Geometric and physical parameters in PEMFC model

Quantity	Value
Gas channel depth	0.5 mm
Gas channel width	1.0 mm
Gas channel length	100 mm
Gas diffusion layer thickness	0.3 mm
Catalyst thickness	0.05 mm
Membrane thickness	0.125 mm
Porosity of gas diffusion layer	0.4
Porosity of catalyst layer	0.28
Permeability of gas diffusion layer	1.76×10^{-11} m^2
Permeability of catalyst layer	1.76×10^{-11} m^2
Permeability of membrane layer	1.18×10^{-18} m^2
Tortuosity of gas diffusion layer	1.5
Tortuosity of catalyst layer	1.5
Electronic conductivity of gas diffusion layer 53 S/m	
Electronic conductivity of catalyst layer 53 S/m	
Inlet temperature	323 K
Operation pressure	1 atm
Anode fuel	H_2, H_2O
Cathode fuel	O_2, N_2
Relative humidity of the anode	100%
Buoyancy (gravity)	−9.81 m/s

Overall, the assumptions made in the current simulations can be summarized as follows:

1. The axial velocity and temperature of the reactant gases are uniformly distributed at the inlet to the gas flow channel.
2. The gases are incompressible and enter the gas flow channel in a direction normal to that of the channel cross-section. The Reynolds number of both fluid flows is less than 200 and the flow is laminar.
3. The GDL, catalyst layer and membrane are all isotropic and homogeneous, and are characterized by high permeability and a uniform porosity.
4. The electrochemical reaction is governed by Butler–Volmer kinetics.
5. The water byproduct of the electrochemical reaction at the cathode side is in a vapor state.
6. The membrane is impervious to the reactant gases.
7. The fuel cell geometry is periodic in the x-axis direction

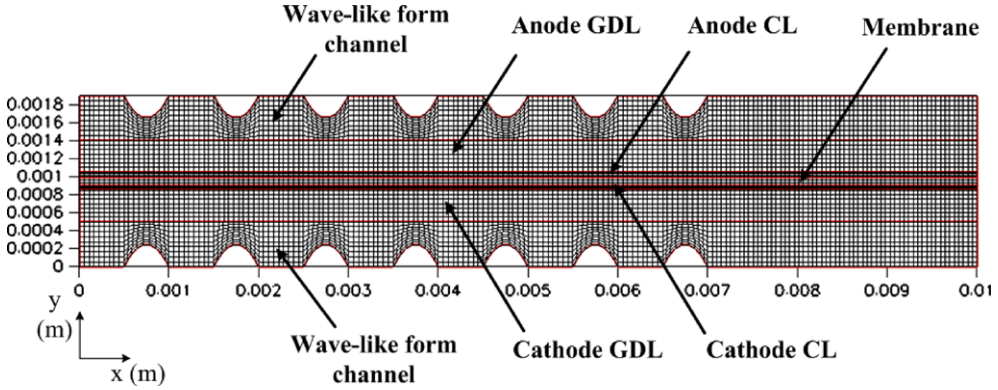

Fig. 2. Computational domain of PEMFC with wave-like gas flow channel.

Table 2
Analytical formulae for source terms in governing equations

	S_u	S_v	S_e	S_c	S_ϕ
Flow channel	0	$g\beta(T-T_{mem})$	0	–	–
Diffusion layer	$-\frac{v\varepsilon^2}{k_p}u-\frac{\varepsilon^3_{eff}C_F\rho u}{\sqrt{k_p}}\sqrt{u^2+v^2}$	$-\frac{v\varepsilon^2}{k_p}v-\frac{\varepsilon^3_{eff}C_F\rho v}{\sqrt{k_p}}\sqrt{u^2+v^2}$	$\rho\frac{i_s^2}{k_s^{eff}}$	0	0
Catalyst layer	$-\frac{v\varepsilon^2}{k_p}u-\frac{\varepsilon^3_{eff}C_F\rho u}{\sqrt{k_p}}\sqrt{u^2+v^2}$	$-\frac{v\varepsilon^2}{k_p}v-\frac{\varepsilon^3_{eff}C_F\rho v}{\sqrt{k_p}}\sqrt{u^2+v^2}$	$\rho j\left[\lvert\eta_{act}\rvert-\frac{T\Delta S}{nF}\right]+\rho\left(\frac{i_m^2}{k_m^{eff}}+\frac{i_s^2}{k_s^{eff}}\right)$	$H_2:-\frac{j_a}{2FC_a}$, $O_2:-\frac{j_c}{4FC_c}$, $H_2O:\frac{j_c}{2FC_c}$	j
Membrane	$-\frac{v\varepsilon^2}{k_p}u-\frac{\varepsilon^2_{eff}C_F\rho u}{\sqrt{k_p}}\sqrt{u^2+v^2}+\frac{k_p}{v}Z_fC_H+F\cdot\nabla\phi\frac{\partial u}{\partial x}$	$-\frac{v\varepsilon^2}{k_p}v-\frac{\varepsilon^2_{eff}C_F\rho v}{\sqrt{k_p}}\sqrt{u^2+v^2}+\frac{k_p}{v}Z_fC_H+F\cdot\nabla\phi\frac{\partial u}{\partial x}$	$\rho\frac{i_m^2}{k_m}$	$\frac{ZF}{RT}D_{k,eff,H^+}\cdot C_{H^+}\left(\frac{\partial^2\phi}{\partial x^2}+\frac{\partial^2\phi}{\partial y^2}\right)$	0

Fig. 2 presents the computational model of the wave-like gas flow channel. For computational efficiency, the domain is divided into seven separate layers, namely the upper wave-like channel, the anode GDL, the anode catalyst layer (CL), the membrane, the cathode CL, the cathode GDL and the lower wave-like channel.

In general, the aim of the gas flow channels in a PEMFC is to maximize the area of the reaction surface exposed to the oxygen and hydrogen reactant gases and to provide a route for the liquid byproduct of the catalytic reaction to flow out of the fuel cell. The wave-like gas flow channel considered in this study has the additional function of enhancing the gas velocity in the vertical direction in order to increase the rate of diffusion of the reactant gases into the catalyst layer.

The heat and mass transfer in the gas flow channels of a PEMFC (both straight channels and those with a wave-like form) can be modeled using conventional mass conservation, Navier–Stokes, and energy and species conservation equations. The basic gas transport equations for a general 2D PEMFC can be expressed as:

Continuity equation:

$$\frac{\partial u}{\partial x}+\frac{\partial v}{\partial y}=0 \tag{1}$$

Momentum equation:

$$\varepsilon_{eff}\left(u\frac{\partial u}{\partial x}+v\frac{\partial u}{\partial y}\right)=-\frac{\varepsilon_{eff}}{\rho}\frac{\partial P}{\partial x}+\upsilon\varepsilon_{eff}\left(\frac{\partial^2 u}{\partial x^2}+\frac{\partial^2 u}{\partial y^2}\right)+S_u \tag{2}$$

$$\varepsilon_{eff}\left(u\frac{\partial v}{\partial x}+v\frac{\partial v}{\partial y}\right)=-\frac{\varepsilon_{eff}}{\rho}\frac{\partial P}{\partial y}+\upsilon\varepsilon_{eff}\left(\frac{\partial^2 v}{\partial x^2}+\frac{\partial^2 v}{\partial y^2}\right)+S_v \tag{3}$$

Energy equation:

$$\varepsilon_{eff}C_p\left(u\frac{\partial T}{\partial x}+v\frac{\partial T}{\partial y}\right)=\frac{k\varepsilon_{eff}}{\rho}\left(\frac{\partial^2 T}{\partial x^2}+\frac{\partial^2 T}{\partial y^2}\right)+S_e \tag{4}$$

Species conservation equation:

$$\varepsilon_{eff}\left(u\frac{\partial C_k}{\partial x}+v\frac{\partial C_k}{\partial y}\right)=D_{k,eff}\left(\frac{\partial^2 C_k}{\partial x^2}+\frac{\partial^2 C_k}{\partial y^2}\right)+S_c \tag{5}$$

Charge conservation equation:

$$\varepsilon_{eff}\left(u\frac{\partial \phi_e}{\partial x}+v\frac{\partial \phi_e}{\partial y}\right)=-S_\phi \tag{6}$$

Table 2 presents the analytical formulae for the source terms S_u, S_v, S_e, S_c and S_ϕ in Eqs. (2)–(6). In these formulae, the parameters ε_{eff}, C_F, k_p and Z_f denote the effective porosity, the quadratic drag factor, the permeability and the valence of the species, respectively. Furthermore, $D_{k,eff}=D_k\varepsilon^{\tau_i}$ represents the effective diffusion coefficient of the kth component of the reactant fuel [23–25].

In a PEMFC, the generation/consumption of the chemical species and the charge transfer take place only in the catalyst layer. Therefore, the source terms in Eqs. (5) and (6) can be implemented based on electrochemical kinetics, i.e.,

$$S_{H_2}=-\frac{j_{anode}}{2F} \tag{7}$$

$$S_{O_2}=-\frac{j_{cathode}}{4F} \tag{8}$$

$$S_{H_2O}=-\frac{j_{cathode}}{2F} \tag{9}$$

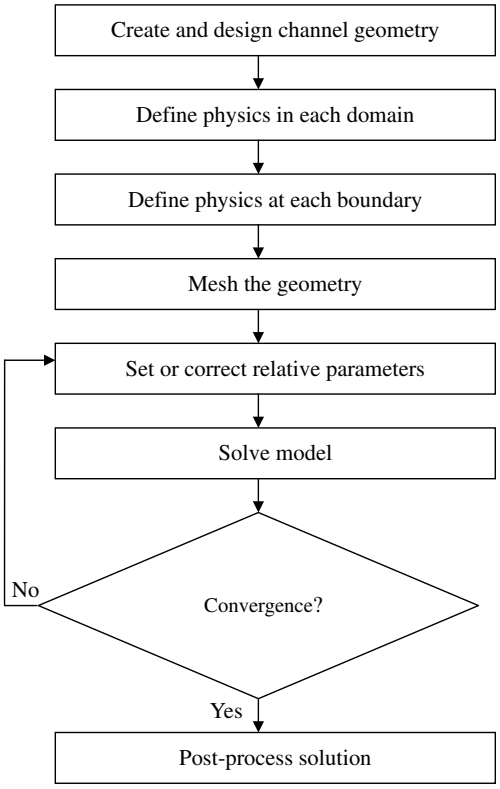

Fig. 3. Flow chart of modeling and simulation procedure.

where j denotes the transfer current density and is derived from the following Butler–Volmer kinetics expressions:

$$j_a = j_{a,ref}\left(\frac{C_{H_2}}{C_{H_2,REF}}\right)^{1/2} \times \left[\exp\left(\frac{\alpha_a F}{RT}\eta_{act}\right) - \exp\left(-\frac{\alpha_c}{RT}F\eta_{act}\right)\right] \quad (10)$$

$$j_c = -j_{a,ref}\left(\frac{C_{O_2}}{C_{O_2,REF}}\right) \times \left[\exp\left(\frac{\alpha_a F}{RT}\eta_{act}\right) - \exp\left(-\frac{\alpha_c}{RT}F\eta_{act}\right)\right] \quad (11)$$

where η_{act} is the surface over potential and is defined as:

$$\eta_{act} = \varphi_{a,c} - \varphi_m - V_{OC} \quad (12)$$

in which $\varphi_{a,c}$ and φ_m denote the potentials of the carbon and membrane phases in the catalyst layer, respectively, and V_{OC} is the reference open-circuit potential of the electrode.

The phase potential equation for the potential and current profile is given by [26,27]:

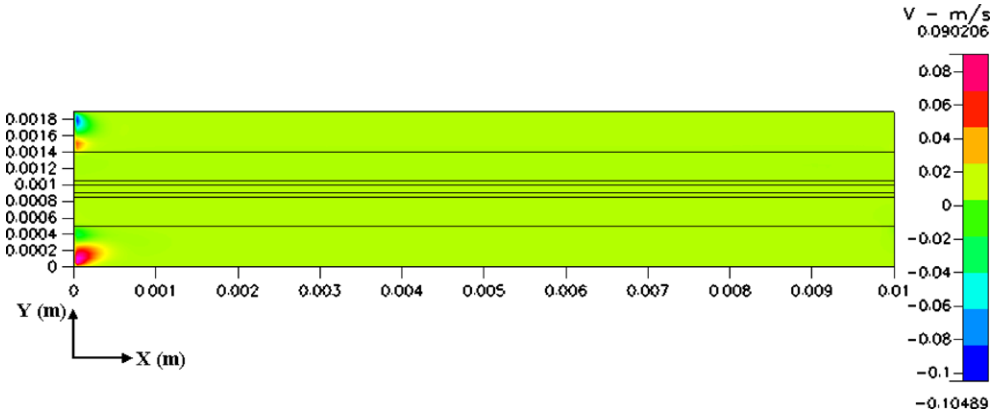

Fig. 4. Velocity field in y-direction in conventional gas flow channel with straight geometry.

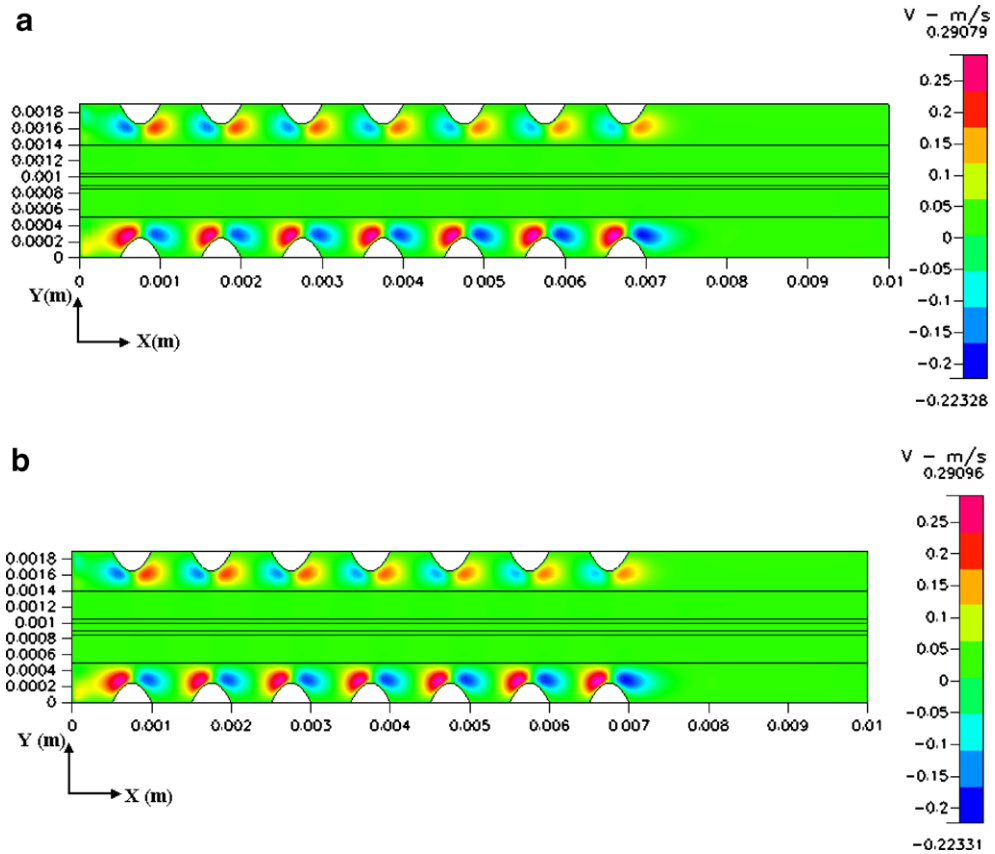

Fig. 5. Velocity field in y-direction in gas flow channel with wave-like configuration. (a) Neglecting buoyancy effects and (b) considering buoyancy effects.

$$\frac{\partial}{\partial x}\left(\sigma_{\mathrm{m}}\frac{\partial \Phi}{\partial x}\right)+\frac{\partial}{\partial y}\left(\sigma_{\mathrm{m}}\frac{\partial \Phi}{\partial y}\right)=S_{\mathrm{j}} \tag{13}$$

where Φ is the phase potential function and σ_{m} is the membrane conductivity, which has the form [3,4]:

$$\sigma_{\mathrm{m}}(T)=\sigma_{\mathrm{m}}^{\mathrm{ref}}\exp\left[1268\left(\frac{1}{303}-\frac{1}{T}\right)\right] \tag{14}$$

where $\sigma_{\mathrm{m,ref}}$ is the reference conductivity of the membrane and is given by:

$$\sigma_{\mathrm{m}}^{\mathrm{ref}}=0.005139\lambda-0.00326 \tag{15}$$

$$\lambda=\left\{\begin{array}{ll}0.043+17.81\cdot a-39.85\cdot a^2+36.0\cdot a^3 & \text{for } 0<a\leqslant 1\\ 14+1.4\cdot(a-1) & \text{for } 1\leqslant a\leqslant 3\end{array}\right\} \tag{16}$$

in which a is the water activity and is defined as:

$$a=\frac{x_{\mathrm{H_2O}}P}{P_{\mathrm{sat}}} \tag{17}$$

In Eq. (17), the saturation pressure varies with the temperature and can be determined directly from thermodynamic tables or from the following empirical expression [28]:

$$P_{\mathrm{sat}}=10^{-2.1794+0.02953T-9.1837\times10^{-5}T^2+1.4454\times10^{-7}T^3} \tag{18}$$

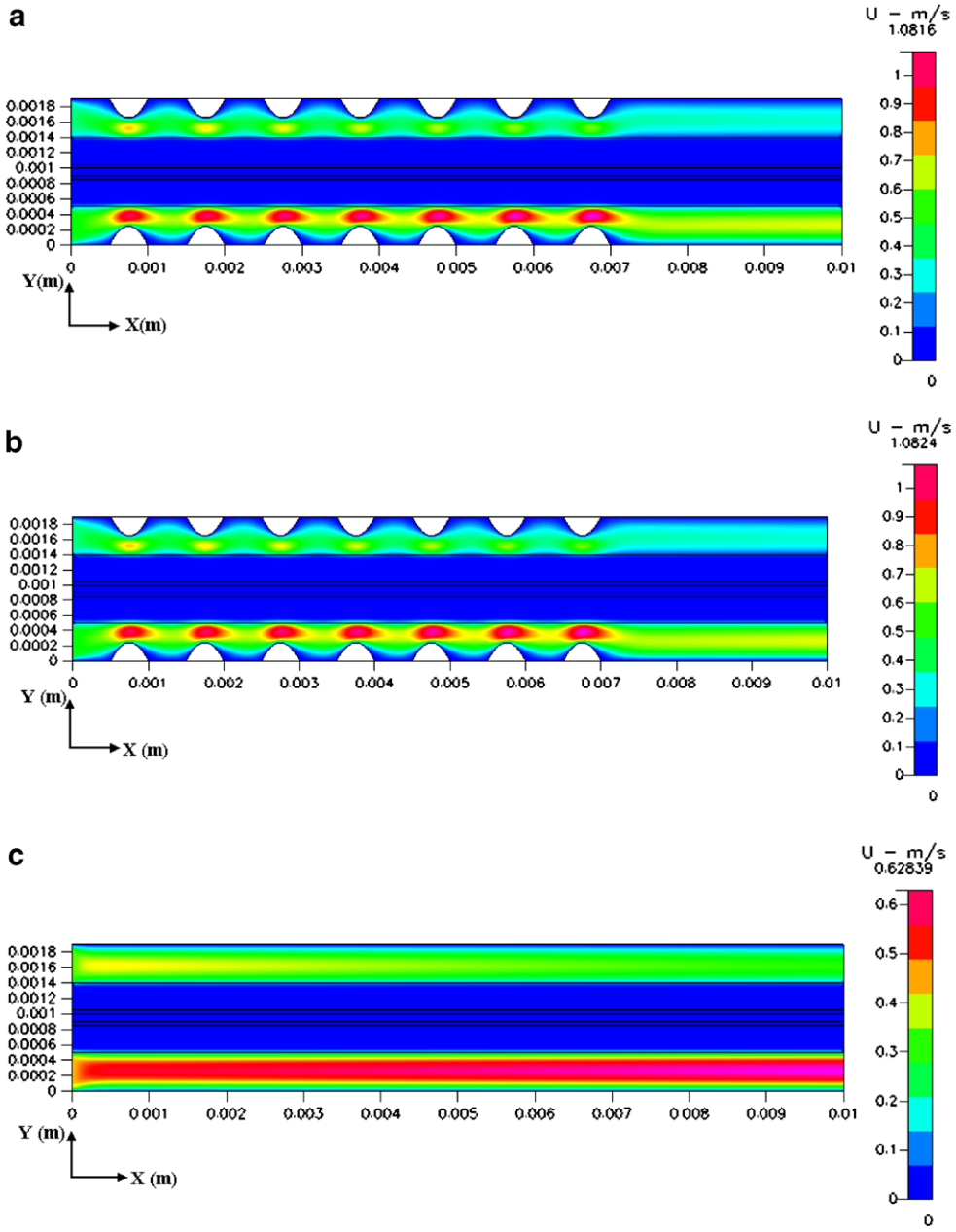

Fig. 6. Velocity field in x-direction in wave-like gas flow channel (with and without buoyancy effects) and straight gas flow channel. (a) Neglecting buoyancy effects, (b) considering buoyancy effects and (c) straight gas flow channel.

3. Boundary conditions

The governing equations for the current PEMFC model are elliptic, partial differential equations. Consequently, boundary conditions are required for all of the boundaries in the computational domain. Due to the conjugated nature of the current problem, the gas flow channel surfaces are included within the solution domain and are treated as fluid of a particular type.

The boundary conditions are as follows:

1. Gas flow channel:

Anode inlet:

$$\begin{aligned} &u = u_{\text{in}}, \quad T = T_{\text{in}} \\ &v = 0, C_{\text{H}_2} = C^{a}_{\text{H}_2,\text{in}}, C_{\text{H}_2\text{O}} = C^{\text{a}}_{\text{H}_2\text{O},\text{in}}, \end{aligned} \tag{19}$$

Cathode inlet:

$$\begin{aligned} &u = u_{\text{in}}, \quad T = T_{\text{in}} \\ &v = 0, C_{\text{O}_2} = C^{\text{c}}_{\text{O}_2,\text{in}}, C_{\text{N}_2} = C^{\text{c}}_{\text{N}_2,\text{in}}, \end{aligned} \tag{20}$$

Interface between gas flow channel walls and GDL:

$$\left.\frac{\partial u}{\partial y}\right|_{y=h_1^-} = \varepsilon_{\text{eff,GDL}} \left.\frac{\partial u}{\partial y}\right|_{y=h_1^+}, \quad \left.\frac{\partial v}{\partial y}\right|_{y=h_1^-} = \varepsilon_{\text{eff,GDL}} \left.\frac{\partial v}{\partial y}\right|_{y=h_1^+} \tag{21}$$

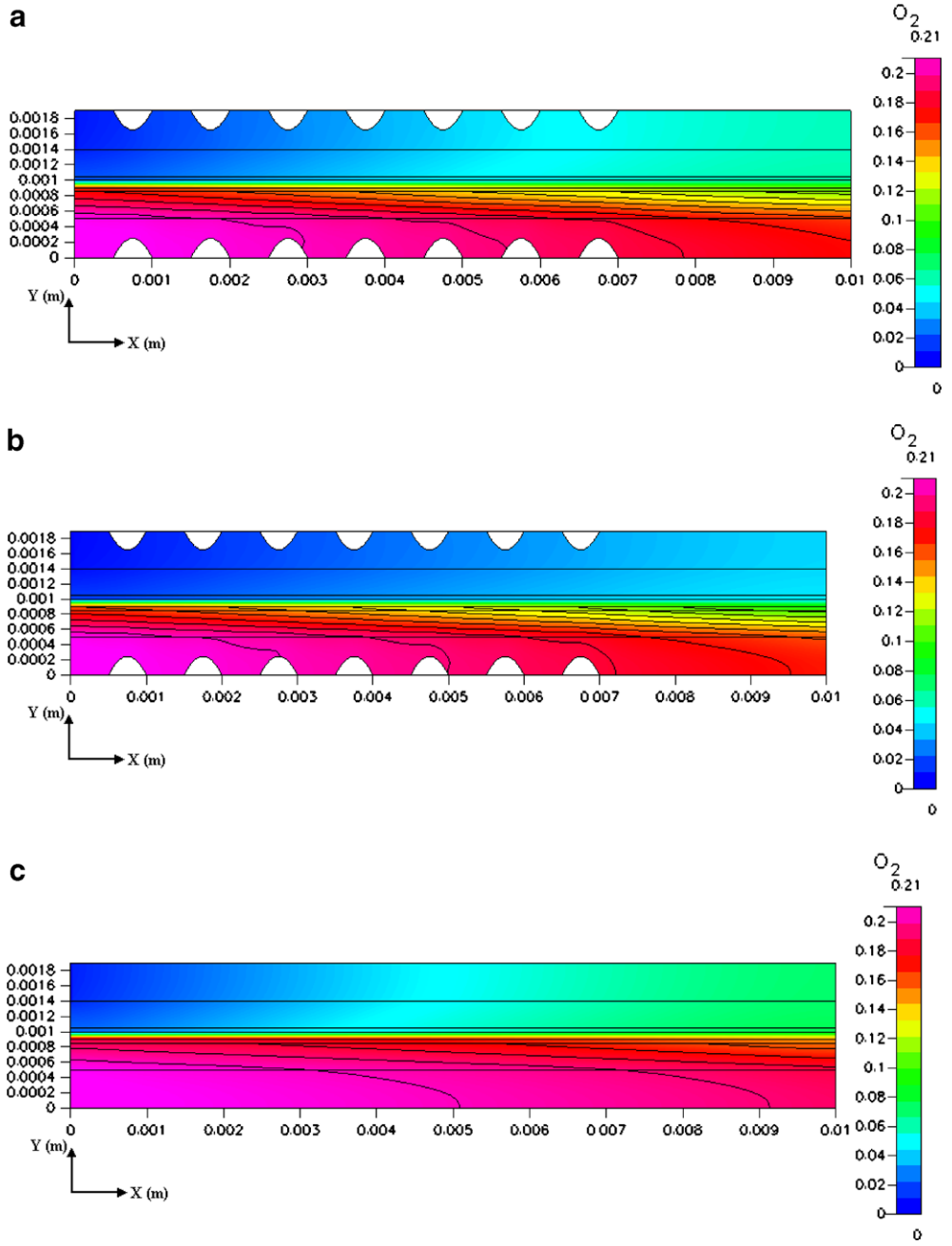

Fig. 7. Oxygen concentration distribution in wave-like gas flow channel (with and without buoyancy effects) and straight gas flow channel for constant cell voltage of 0.6 V. (a) Neglecting buoyancy effects, (b) considering buoyancy effects and (c) straight type gas flow channel.

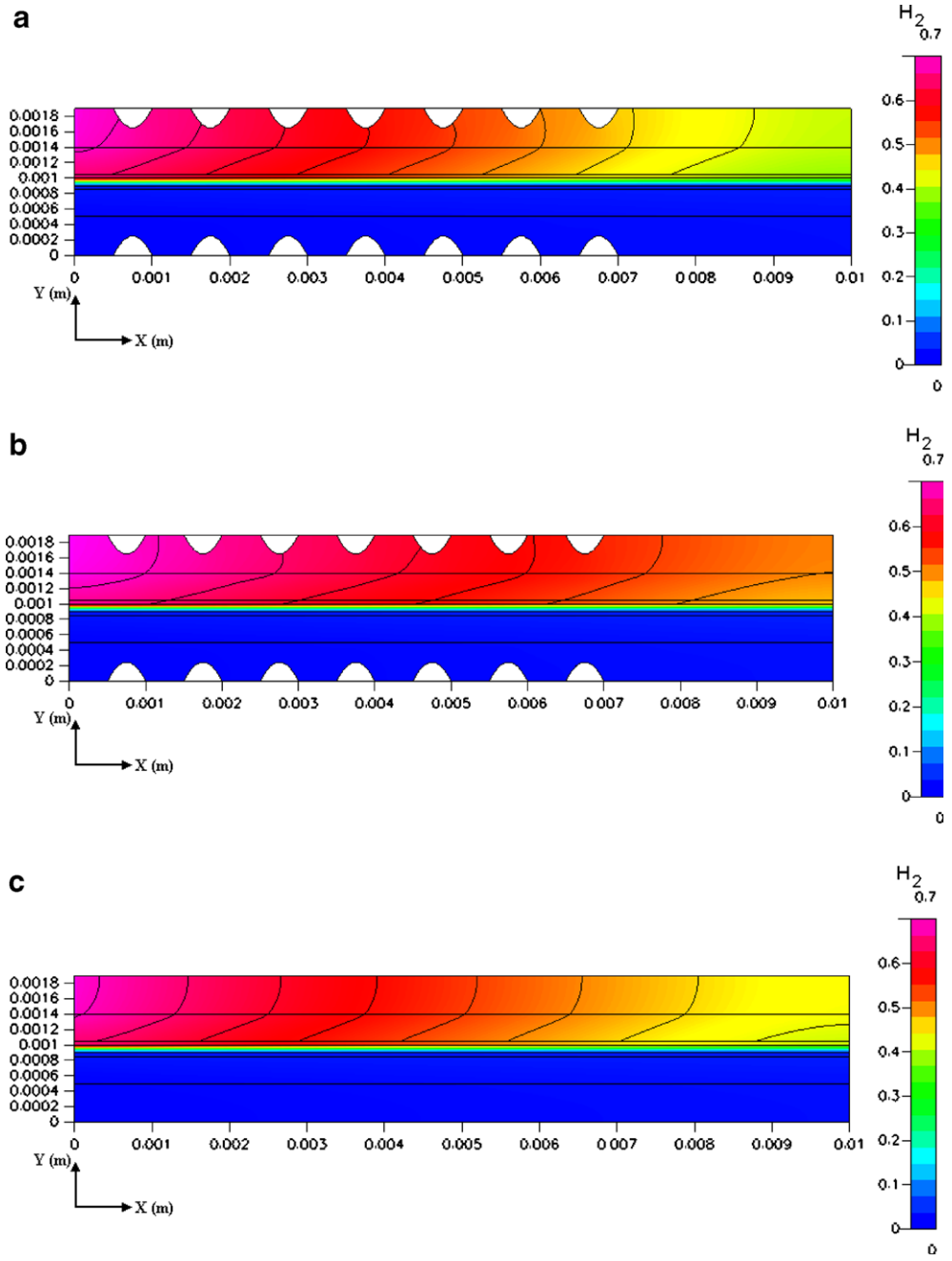

Fig. 8. Hydrogen concentration distribution in wave-like gas flow channel (with and without buoyancy effects) and straight gas flow channel for constant cell voltage of 0.6 V. (a) Neglecting buoyancy effects, (b) considering buoyancy effects and (c) straight type gas flow channel.

Interface between GDL and catalyst layer:

$$\varepsilon_{\text{eff,GDL}} \left.\frac{\partial u}{\partial y}\right|_{y=h_2^-} = \varepsilon_{\text{eff,CL}} \left.\frac{\partial u}{\partial y}\right|_{y=h_2^+},$$
$$\varepsilon_{\text{eff,GDL}} \left.\frac{\partial v}{\partial y}\right|_{y=h_2^-} = \varepsilon_{\text{eff,CL}} \left.\frac{\partial v}{\partial y}\right|_{y=h_2^+} \quad (22)$$

Interface between catalyst layer and membrane:

$$u = v = C_{\text{k}} = 0 \quad (23)$$

2. Gas flow channel outlet:

$$\frac{\partial u}{\partial x} = \frac{\partial v}{\partial x} = \frac{\partial T}{\partial x} = 0 \quad (24)$$

3. Upper surface:

Anode gas channel:

$$u = v = 0 \quad (25)$$
$$T_{\text{surface}} = 298\text{K} \quad (26)$$

4. Lower surface:

Cathode gas channel:

$$u = v = 0 \quad (27)$$

$$T_{\text{surface}} = 298\text{K} \quad (28)$$

$$T_{\text{in}} > T_{\text{w}} \quad (29)$$

4. Numerical method

Fig. 3 presents a flow chart of the current numerical modeling procedure. The simulations are performed using the commercial CFD–RC software package, which discretizes the mass, momentum, energy and species concentration equations using the finite-volume SIMPLEC (semi-implicit method for pressure-linked equations consistent) method [29]. The various models in CFD–ACE are fully described in [30]. In the simulations, it is assumed that the inlet section of the channel is fully developed hydro-dynamically. Hence, a fully-developed velocity profile for rectangular ducts is imposed. Additionally, a forced convection regime [31,32] is imposed within the computational domain and the Navier–Stokes equations are solved under laminar assumptions. Prior to the simulations, a parametric study was performed to identify a suitable grid mesh capable of generating accurate representations of the thermal and velocity gradients near the walls so as to provide detailed insights into the electrochemical reaction and mass transport phenomena in the PEMFC. A spatial resolution of 200 × 40 meshes was found to be sufficient, with a fine mesh size used throughout the computational domain. In the simulations, the iterative computations were terminated once the value of the residues fell to less than 10^{-6}. The computations were performed using a PC with a 3.2 GHz Intel Pentium 4 CPU, 1 GB DDR RAM and the Windows XP operating system.

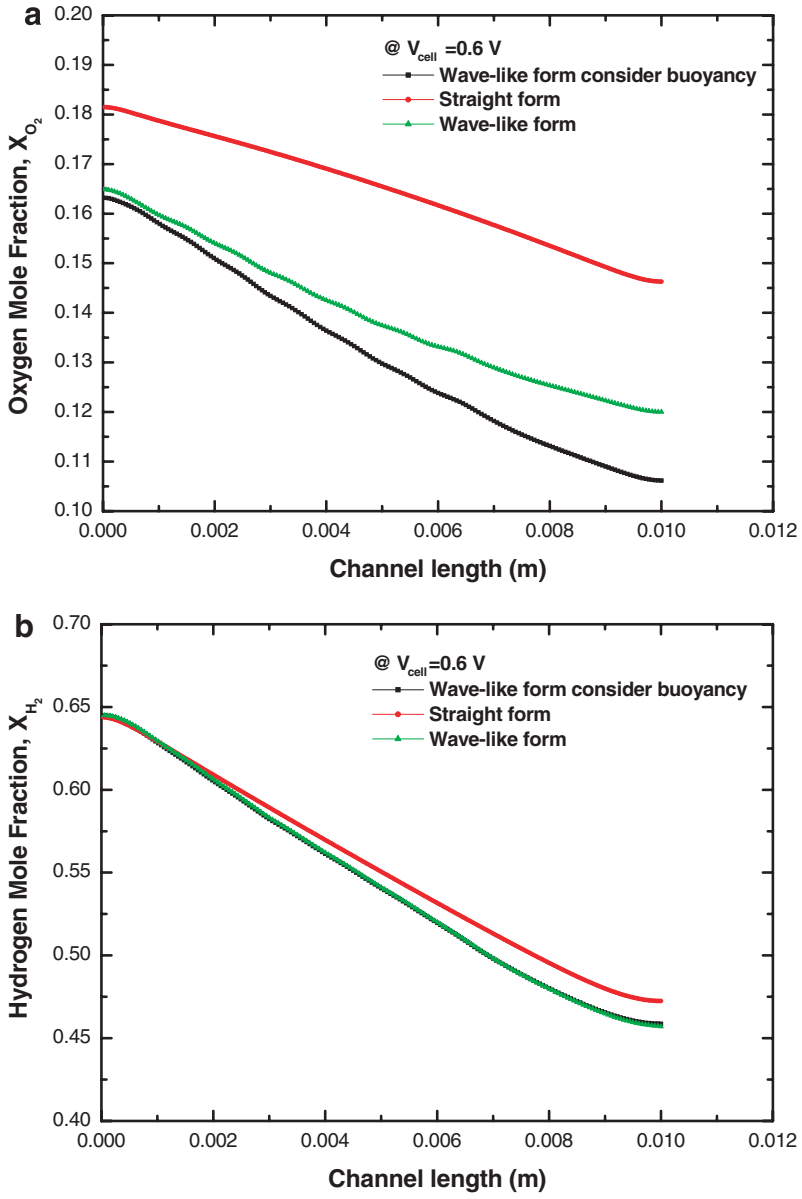

Fig. 9. Variation in oxygen and hydrogen mole fraction profiles in catalyst layers as function of channel length in wave-like gas flow channel (with and without buoyancy effect) and straight gas flow channel at operating cell potential of 0.6 V. (a) Oxygen concentration and (b) hydrogen concentration.

5. Results and discussion

5.1. Velocity field

The fluid flow in the wave-like gas flow channel has an axial velocity component (u) and a vertical velocity component (v). Fig. 4 shows the vertical velocity distribution in a straight gas flow channel under the following operating conditions: (1) a cell potential of 0.6 V, (2) a cathode gas flow inlet velocity of 0.4 m/s, and (3) an anode gas flow inlet velocity of 0.2 m/s. Fig. 5 illustrates the vertical velocity profiles of the flow in a wave-like gas flow channel under the same operating conditions. Note that the upper panel presents the velocity distribution for the case in which the buoyancy effects are neglected, while the lower panel shows the velocity distribution when the effects of buoyancy are considered. Comparing Figs. 4 and 5, it is apparent that the periodic wave-like structure of the gas flow channel increases the velocity in the vertical direction. The increased supply of reactant gases to the catalyst layer enhances the efficiency of the catalytic reaction and therefore improves the performance of the PEMFC. Fig. 6 presents the distributions of the axial flow velocity in the wave-like gas flow channel (with and without buoyancy effects) and in the straight gas flow channel. The results of Figs. 5 and 6 reveal that the inclusion of buoyancy effects when modeling the fluid behavior in the wave-like gas flow channel increases the maximum y-direction velocity from 0.2908 m/s to 0.2910 m/s and increases the maximum x-direction velocity from 1.0816 m/s to 1.0824 m/s. In general, it is observed that the velocity is higher in the wave-like channel than in the straight channel because the constricted channel area above each crest in the wave-like channel surface generates a nozzle-type effect which accelerates the flow. However, Fig. 6 shows that the axial velocity of the reactant gases reduces in the trough regions of the wave-like channel. This has the effect of trapping the fuel in these particular regions of the channel, thereby further increasing the supply of fuel to the catalyst layer. Figs. 5 and 6 also show that a strong convection force is induced along the reaction surface of the wave-like gas flow channel. This not only increases the supply of the reactant gases to the catalyst layers, but also improves the flow of the reaction byproducts out of the PEMFC. Thus, the performance of the fuel cell is significantly improved, particularly at higher current densities.

5.2. Concentration distribution

Figs. 7 and 8 show the oxygen and hydrogen concentrations in the wave-like gas flow channels (with and without buoyancy effects) and in the straight gas flow channel. Note that in both figures, the cathode over potential is 0.6 V and the color-coded scale indicates the normalized concentration of the reactant gases. In general, the figures show that both gas concentrations reduce slightly along the axial

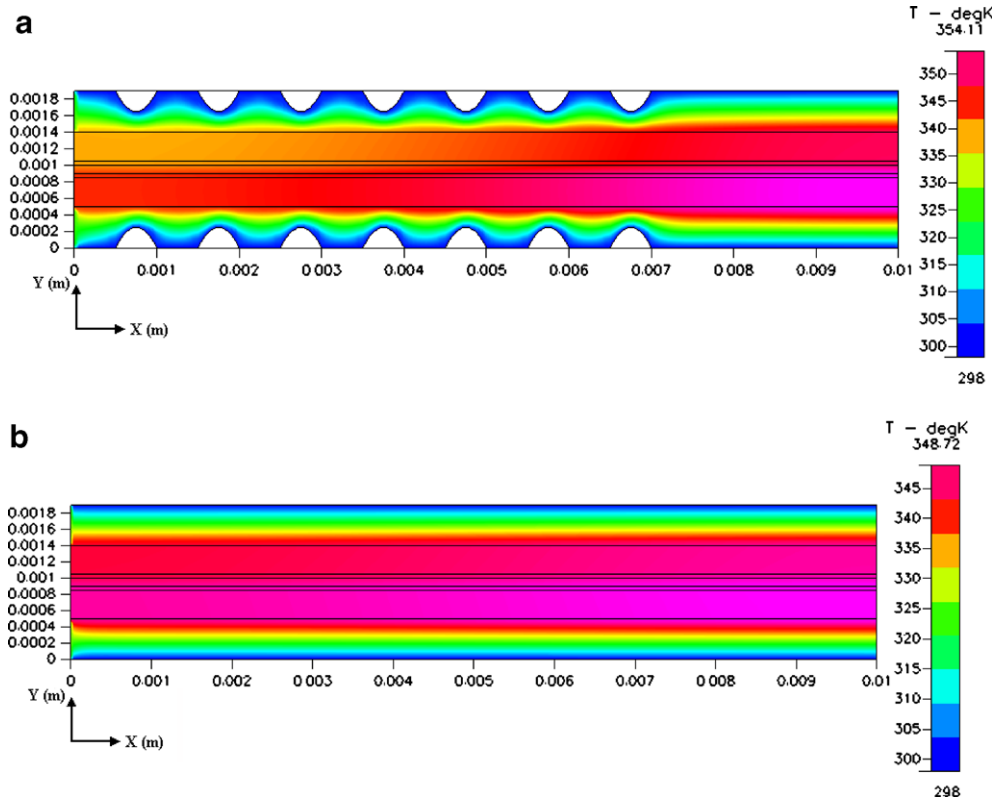

Fig. 10. Temperature field in wave-like gas flow channel and straight gas flow channel for inlet temperature of 323 K (50 °C). (a) Wave-like geometry and (b) straight geometry.

direction of the two channels. Furthermore, it is observed that the oxygen concentration in the wave-like gas flow channel varies significantly in the GDL region, particularly near the reaction surface. By contrast, in the straight channel, the oxygen concentration remains relatively uniform. The greater variation in the oxygen concentration in the wave-like gas channel is caused by a forced convection effect in the diffusion layer.

Fig. 9 illustrates the variation in the oxygen and hydrogen mole fractions in the axial direction of the wave-like gas flow channel (with and without buoyancy effects) and the straight gas flow channel. Note that the operating voltage is assumed to be 0.6 V in every case. It is apparent that both the oxygen fraction and the hydrogen fraction decrease along the axial direction as the two reactant gases are consumed in the catalyst layers. Furthermore, it can be seen that the consumption of the reactant gases is more pronounced in the wave-like gas flow channel than in the straight channel. This phenomenon is attributable to the enhanced y-direction velocity flow component in the wave-like channel, which drives the gases through the diffusion layer into the catalyst layers. Finally, it is observed that the buoyancy force has virtually no effect on the consumption of hydrogen, but increases the consumption of oxygen considerably. The effect of the buoyancy force on the oxygen consumption becomes increasingly apparent as the oxygen flows further along the channel.

5.3. Temperature field

Fig. 10 shows the temperature distribution in the wave-like gas flow channel and the straight gas flow channel,

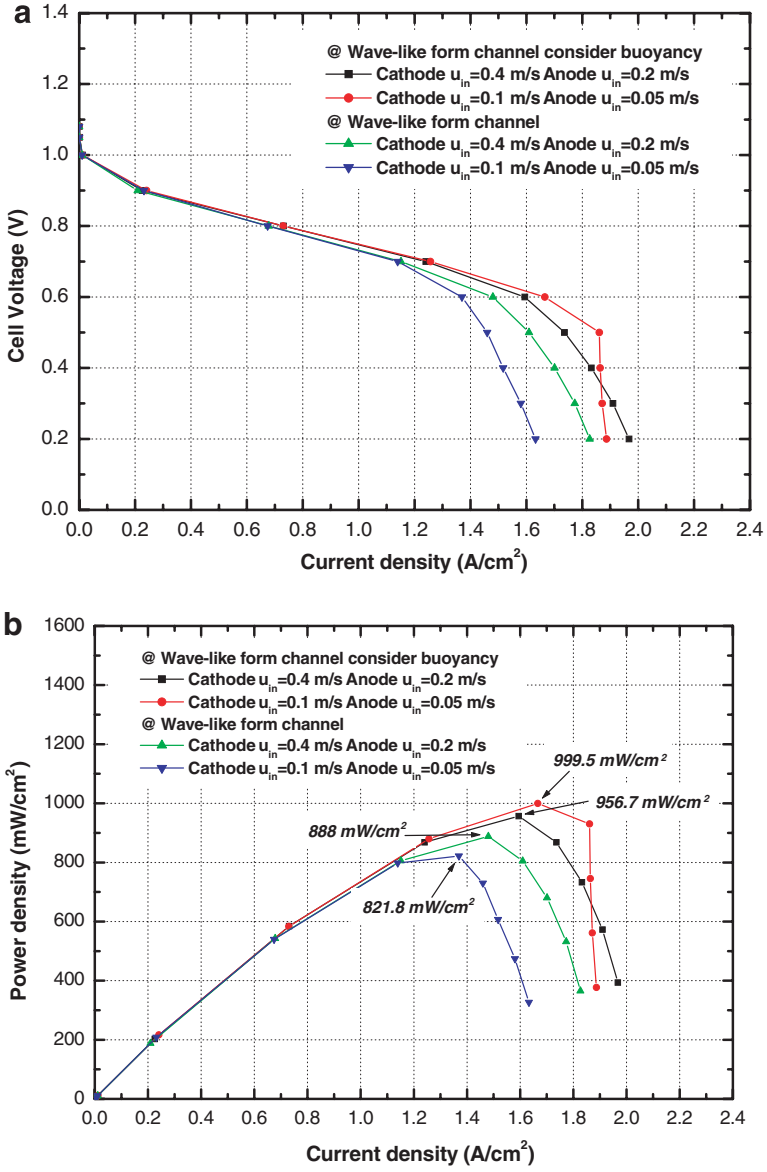

Fig. 11. (a) Polarization curve and (b) power density curve in wave-like gas flow channels (with and without buoyancy effects) for various inlet velocity conditions.

respectively, for a cathode gas inlet velocity of 0.4 m/s and an anode gas inlet velocity of 0.2 m/s. It is seen that the wave-like channel results in a lower and more uniform temperature distribution within the channel. In other words, the wave-like gas flow channel improves the heat transfer performance of the PEMFC and reduces the cell reaction temperature. In general, the improvement obtained in the single-phase convective heat transfer performance in the gas flow channel may be the result of an increased flow interruption, a reduction in the thermal boundary layer, or an increased velocity gradient near the GDL boundary.

5.4. Polarization curve

Fig. 11 presents the variation in the cell voltage and the power density as a function of the current density for wave-like gas flow channels both with and without buoyancy effect considerations. In general, the results show that the cell voltage increases when the buoyancy effect is taken into consideration. Furthermore, for a cathode inlet velocity of 0.4 m/s and an anode velocity of 0.2 m/s, the inclusion of the buoyancy effect increases the maximum power density by 7.7%, i.e. from 888 mW/cm^2 to 956.7 mW/cm^2. When the cathode and anode inlet velocities are reduced to 0.1 m/s and 0.05 m/s, respectively, the buoyancy effect increases the computed value of the maximum power density from 821.8 mW/cm^2 to 999.5 mW/cm^2; an increase of 21.6%. The results show that a lower inlet velocity of the two reactant gases increases the power density, but results in a cell voltage drop since the reactant gases are not replaced sufficiently quickly once they have been consumed in the reaction process. Nonetheless, the upper panel in

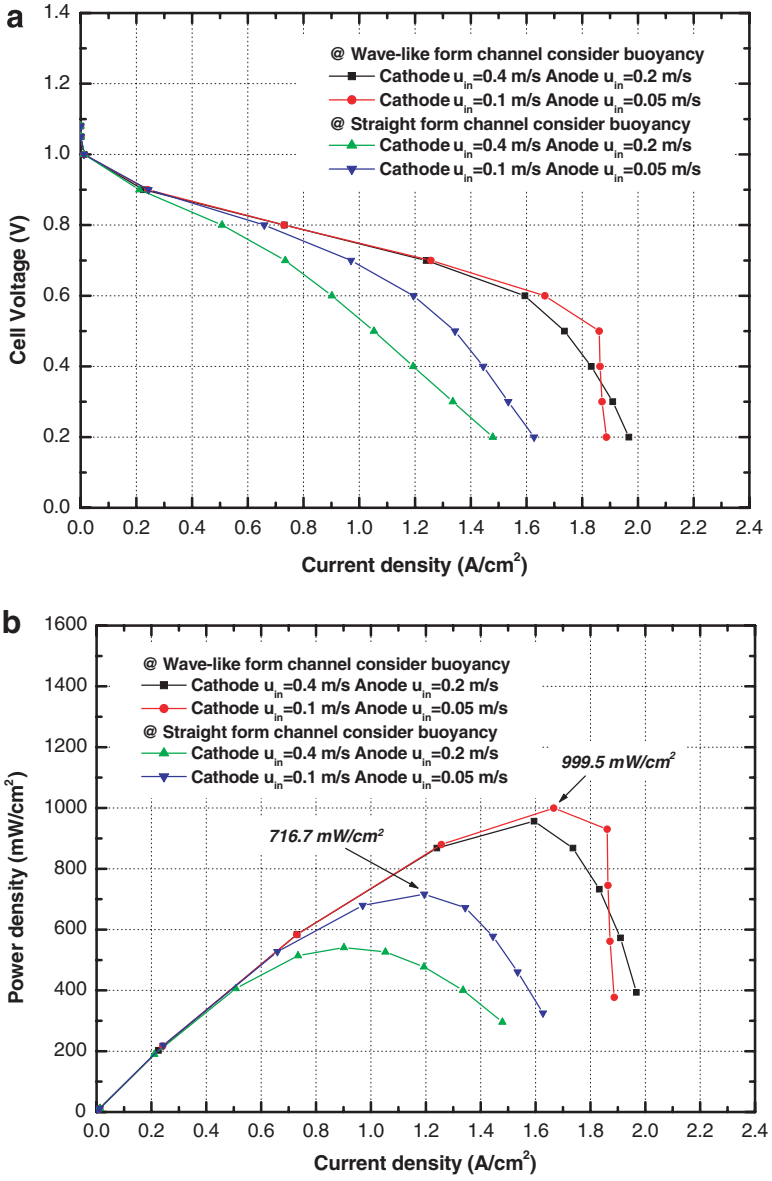

Fig. 12. (a) Polarization curve and (b) power density curve in wave-like gas flow channel (with buoyancy effects) and straight gas flow channel for various inlet velocity conditions.

Fig. 11 shows that the buoyancy force is instrumental in overcoming the effects of these mass transport losses.

The polarization characteristics of a PEMFC provide a convenient means of evaluating the performance of fuel cells with different gas flow channel configurations. Fig. 12 shows the polarization and power density curves of PEMFCs with wave-like gas flow channels and straight gas flow channels, respectively. Note that the results presented for the wave-like gas flow channels are computed with buoyancy force effects taken into account. It is seen that for an oxygen inlet velocity of 0.4 m/s and a hydrogen inlet velocity of 0.2 m/s, the PEMFC with a wave-like gas channel yields a higher cell voltage and power density than the conventional gas channel with a straight configuration. When the oxygen and hydrogen inlet velocities are reduced to 0.1 m/s and 0.05 m/s, respectively, both PEMFCs have a slightly poorer performance. However, the performance of the PEMFC with a wave-like gas flow channel is better than that of the PEMFC with a straight channel since the wave-like surface increases the supply of oxygen to the reaction layer. From inspection, it is found that the maximum power density of the PEMFC with a wave-like gas flow channel is approximately 39.5% higher than that of the PEMFC with the straight channel. This result indicates that the wave-like surface of the flow channel changes the transport of the reactant gas to the catalyst layer surface from a solely diffusion-based mechanism to a convection mechanism, and leads to a significantly improved electrical performance as a result.

6. Conclusions

This study has developed a two-dimensional computational model to study the fluid flow phenomena in PEMFCs with wave-like gas flow channels and conventional straight gas flow channels, respectively. The heat transfer performance and gas flow velocity characteristics of the two different channel geometries have been examined. Furthermore, the effects of buoyancy forces in the gas flow channel on the gas flow characteristics, the temperature distribution, the electrochemical reaction efficiency and the electrical performance of the PEMFC have been analyzed. In general, the results have shown that compared to a conventional gas flow channel, the wave-like channel provides a significantly improved convective heat transfer performance and a higher gas flow velocity, which in turn improves the efficiency of the catalytic reaction. The improvement in the catalytic reaction efficiency is particularly apparent when the buoyancy effect is taken into consideration. Compared with a conventional PEMFC with a straight gas flow channel, the PEMFC with a wave-like gas flow channel has considerably improved current density and polarization characteristics; particularly at lower inlet velocities of the two reactant gases. Specifically, the numerical results show that the wave-like configuration improves the maximum power density by approximately 39.5%.

Acknowledgement

This research was supported by the National Science Council of Taiwan under Contract No. NSC 94-2212-E-006-019.

References

[1] D.M. Bernardi, M.W. Verbrugge, Mathematical model of a gas diffusion electrode bonded to a polymer electrolyte, AIChE Journal 37 (1991) 1151–1163.
[2] D.M. Bernardi, M.W. Verbrugge, A mathematical model of the solid-polymer–electrolyte fuel cell, J. Electrochem. Soc. 139 (1992) 2477–2491.
[3] T.E. Springer, T.A. Zawodzinski, S. Gottesfeld, Polymer electrolyte fuel cell model, J. Electrochem. Soc. 136 (1991) 2334–2342.
[4] T.V. Nguyen, R.E. White, A. Water, A water and heat management model for proton-exchange-membrane fuel cells, J. Electrochem. Soc. 140 (1993) 2178–2186.
[5] J.K. Kuo, C.K. Chen, A novel Nylon-6-S316L fiber compound material for injection molded PEM fuel cell bipolar plates, J. Power Sources 162 (2006) 207–214.
[6] J.K. Kuo, C.K. Chen, Evaluating the enhanced performance of a novel wave-like form gas flow channel in the PEMFC using the field synergy principle, J. Power Sources 162 (2006) 1122–1129.
[7] C.K. Chen, J.K. Kuo, Nylon 6/CB polymeric conductive plastic bipolar plates for PEM fuel cells, J. Appl. Polym. Sci. 101 (2006) 3415–3421.
[8] Y.T. Yang, C.K. Chen, M.T. Lin, Natural convection of non-Newtonian fluid effect, Int. J. Heat Mass Transfer 39 (1996) 2831–2842.
[9] E. Kim, Natural convection along a wavy vertical plate to non-Newtonian fluids, Int. J. Heat Mass Transfer 40 (1997) 3069–3078.
[10] C.C. Wang, C.K. Chen, Forced convection in a wavy-wall channel, Int. J. Heat Mass Transfer 45 (2002) 2587–2595.
[11] C.Y. Wang, P. Cheng, A multiphase mixture model for multiphase, multicomponent transport in capillary porous media–I. Model development, Int. J. Heat Mass Transfer 39 (1996) 3607–3618.
[12] Z.H. Wang, C.Y. Wang, K.S. Chen, Two-phase flow and transport in the air cathode of proton exchange membrane fuel cells, J. Power Sources 94 (2001) 40–50.
[13] J. Yuan, M. Rokni, B. Sunden, Simulation of fully developed laminar heat and mass transfer in fuel ducts with different cross-sections, Int. J. Heat Mass Transfer 44 (2001) 4047–4058.
[14] L. You, H. Liu, A two-phase flow and transport model for the cathode of PEM fuel cells, Int. J. Heat Mass Transfer 45 (2002) 2277–2287.
[15] J. Yuan, M. Rokni, B. Sunden, Three-dimensional computational analysis of gas and heat transport phenomena in ducts relevant for anode-supported solid oxide fuel cells, Int. J. Heat Mass Transfer 46 (2003) 809–821.
[16] S. Mazumder, J.V. Cole, Rigorous 3-D mathematical modeling of PEM fuel cells I. Model proditions without liquid water transfer, J. Electrochem. Soc. 150 (2003) 1510–1517.
[17] G. Hu, J. Fan, S. Chen, Y. Liu, K. Cen, Three-dimensional numerical analysis of proton exchange membrane fuel cells (PEMFCs) with conventional and interdigitated flow fields, J. Power Sources 136 (2004) 1–9.
[18] C.Y. Wang, Fundamental models for fuel cell engineering, Chem. Rev. 104 (2004) 4727–4766.
[19] W.M. Yam, H. C Liu, C.Y. Soong, F. Chen, C.H. Cheng, Numerical study on cell performance and local transport phenomena of PEM fuel cells with novel flow field designs, J. Power Sources 161 (2006) 907–919.
[20] A. Omri, S.B. Nasrallah, Control volume finite element numerical simulation of mixed convection in air-cooled cavity, Numer. Heat Transfer A: Appl. 36 (6) (1999) 615–637.

[21] H. Jasak, A.D. Gasman, Automatic resolution control for the finite-volume method, part 1: A-posteriori error estimates, Numer. Heat Tr B: Fund. 38 (3) (2000) 237–256.
[22] E. Chenier, R. Eymard, O. Touazi, Numerical results using a collocated finite-volume scheme on unstructured grids for incompressible fluid flows, Numer. Heat Transfer B: Fund. 49 (3) (2006) 259–276.
[23] C.I. Lee, H.S. Chu, Effects of cathode humidification on the gas–liquid interface location in a PEM fuel cell, J. Power Sources 161 (2006) 949–956.
[24] J.J. Hwang, C.H. Chao, W.Y. Ho, C.L. Chang, D.Y. Wang, Effect of flow orientation on thermal–electrochemical transports in a PEM fuel cell, J. Power Sources 157 (2006) 85–97.
[25] J.J. Hwang, P.Y. Chen, Heat/mass transfer in porous electrodes of fuel cells, Int. J. Heat Mass Transfer 49 (2006) 2315–2327.
[26] K. Vafai, C.L. Tien, Boundary and inertial effects on flow and heat transfer in porous media, Int. J. Heat Mass Transfer 24 (1981) 152–169.
[27] T.C. Jen, T. Yan, S.H. Chan, Chemical reacting transport phenomena in a PEM fuel cell, Int. J. Heat Mass Transfer 46 (2003) 4157–4168.
[28] H.C. Liu, W.M. Yan, C.Y. Soong, F. Chen, Effects of baffle-blocked flow channel on reactant transport and cell performance of a proton exchange membrane fuel cell, J. Power Sources 142 (2005) 125–133.
[29] S.V. Patankar, Numerical Heat Transfer and Fluid Flow, Hemisphere/McGraw-Hill, New York, 1980.
[30] CFD Research Corp., CFD-ACE (U)^{TM} User Manual, version, Huntsville, Alabma (2002).
[31] P.L. Woodfield, K. Suzuki, K. Nakabe, Performance of a three-dimensional, pressure based, unstructured finite-volume method for low-reynolds-number incompressible flow and wall heat transfer rate prediction, Numer. Heat Transfer B: Fund. 43 (5) (2003) 403–423.
[32] D.N. Pope, G. Gogos, A new multi-component diffusion formulation for the finite-volume method: Application to convective droplet combustion, Numer. Heat Transfer B: Fund. 48 (3) (2005) 213–233.